Measurements of Scintillation over a 17.55km Horizontal Path

M Bernhardt[1], J Buckle[1], J C Dainty[2], F Reavell[2], V Ruiz-Cortes[2], M Welch[1] and N J Wooder[2].

[1] SASD Division, DERA, Farnborough GU14 0LX, UK.

[2] Blackett Laboratory, Imperial College, London SW7 2BZ, UK

ABSTRACT

An extensive set of measurements of scintillation over a 17.55km path have been made using point sources at wavelengths of 633nm and 10.6μm, and using an extended thermal source at 3-5μm and 8-12μm. The basic data consists of normalised variances, probability histograms and normalised autocorrelation functions of intensity. The main aim was to produce a set of data that might be used as inputs to models for scintillation. The measurements, as expected, showed a very large range of observed fluctuations, with a highest recorded normalised variance at 633nm of $\approx$34 and an average value of 4.8 (averaged over 130 data sets), with a standard deviation of 4.1. The probability histograms have been fitted using log-normal, exponential, log-normally modulated exponential and K distributions. As a general rule, the log-normal model gives a good fit in a large number of cases. Power spectra and correlations functions were measured and show the expected trends with wavelength, with average correlation times (defined in the text) in the range 10 msec (visible) to 68 msec (CO_2).

Keywords: Scintillation, Propagation

1. INTRODUCTION

Although a number of experimental studies of atmospheric scintillation have been conducted over the past two decades,[1–7] few measurements over very long horizontal paths have been reported in the open literature. An ideal measurement programme would involve simultaneous measurement of both atmospheric properties such as temperature fluctuations and the optical properties of the wave that has propagated through the turbulence. The most complete set of measurements in this regard was made by Consortini et al[3] over a 1.2km path. In the case of a very long path, it is probably impractical to make simultaneous atmospheric and optical measurements, yet the optical measurements in themselves may be useful, both for empirical models and to stimulate further theoretical analysis. The key feature of very long path measurements is that the observed fluctuations of intensity may be *very* large: for example, in the present study, we observed, at $\lambda = 633$nm, a mean normalised variance of 4.8 $\pm$4.1, with occasional values (measured over $\approx$150s) exceeding 10. These extreme values present a challenge to theoreticians and numerical modellers, even though we cannot specify the exact atmospheric conditions during the measurement.

In the present study, several light sources were placed approximately 17.55km from the detection location: these included slightly diverging He-Ne ($\lambda = 633$nm) and CO_2 (λ =10.6μm) laser sources an a 750mm diameter thermal source. The scintillation was measured at three wavelengths: 633nm (laser source only), 3-5μ (thermal source only) and 8-12μm (laser and thermal souces) using telescope optics and integration apertures of 6mm (visible) and 150mm (infrared).

2. DESCRIPTION OF EQUIPMENT

The equipment used for the measurements of scintillation consists of three parts: (i) source assembly, (ii) detector system and (iii) a data acquisition and processing system.

2.1. Source Assembly

This is shown schematically in Figure 1. The output of the CO_2 laser (air cooled Synrad 48-1-28 with a rated output of 10W) is fed to a -19mm focal length (at 10.6μm) ZnSe diverging lens via two beam steering mirrors M_1, M_2 and the dichroic beam combiner. The output of the HeNe laser (Uniphase 1135 of minimum rated output of 10mW) is fed to the same ZnSe lens (the focal length at 633nm is -16.7mm) via the steering mirror M_3 and the beam combiner. The resulting coaxial diverged beams are fed to the 750mm focal length off axis paraboloid to form the

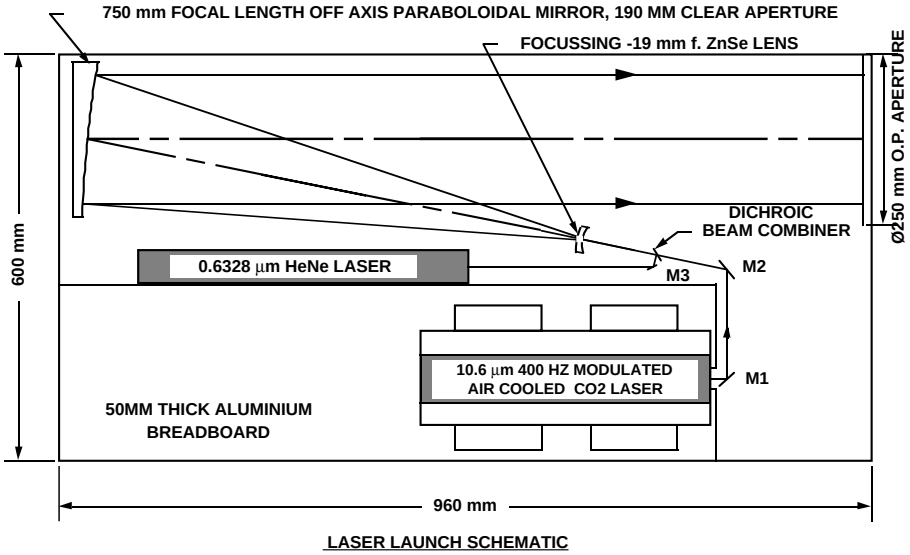

Figure 1. Laser source optics.

output beams. The equipment is mounted on a 600 × 1200 × 50mm aluminium breadboard which has a pointing sensitivity of approximately 3 arc seconds. A framework holds and protects the assembly in inclement weather.

The thermal source is a US military search light parabolic mirror with a globar at the focus. The mirror has a 750mm diameter aperture. The source is an industrial gas clothes drier ignitor (cost ≈ $25). It is estimated that the surface temperature of this source is in the region of 1600degK at its rated applied voltage of 110 volts ac (approximately 380 watts). A hyperboloid was machined and was placed near the rear of the paraboloid, converting the system to a Cassegrain configuration. The numerical aperture was reduced by a factor of 25 but this was compensated by the larger area of the source used. This arrangement allowed us to chop the beam for background rejection.

2.2. Receiver System

The receiver system is shown schematically in Figure 2. The equipment is mounted on a 600 × 900 × 50mm foam filled aluminium optical breadboard. This is kinematically mounted on an angle-iron frame similar to that for the launch optics.

Light is collected by a Cassegrain telescope made up of an f=600mm, 150mm diameter parabolic primary and an f=250mm, 50mm diameter spherical secondary: the actual focal length is 2100mm. This gives a wavefront aberration of 3λ at 0.633m and $\lambda/6$ at 10.6m at full aperture. A Graseby CMT & InSb two colour detector 2C-1 with 1mm × 1mm elements is placed at the Cassegrain focus. XY slides allow centring the position of the image on this detector. The detector is fed to Graseby preamps DP-8000 and DP-8100. The field-of-view has been factory reduced to 5deg.

A dichroic beam splitter picks off the visible fraction of the light from the telescope and is collimated using f=120mm doublet. After turning the collimated beam back along the optical breadboard the beam is imaged with an f=140mm lens onto an Electron Tubes 9130B/100 30mm S20 cathode photon counting photomultiplier. A 1nm bandwidth 633nm filter is used to reject the non-HeNe radiation. A variable aperture stop is placed at the image of the telescope pupil plane to reduce the aperture in the visible: this plane has a magnification of 1/18 of the entrance pupil of the Cassegrain telescope, so that a standard 0.33mm aperture has a diameter in the entrance pupil of approximately 6mm. A neutral density filter wheel is also supplied near this plane to vary the light reaching the photomultiplier. A selector mirror just before the aperture stop allows a Pulnix TM-765 TV camera or eyepiece to be selected for visual observation of the telescope image. All the optics are covered in to reject all light other than that through the telescope aperture. These light shields are coated on the interior with Nextel Velvet Black.

Send correspondence to J C Dainty E-mail: c.dainty@ic.ac.uk

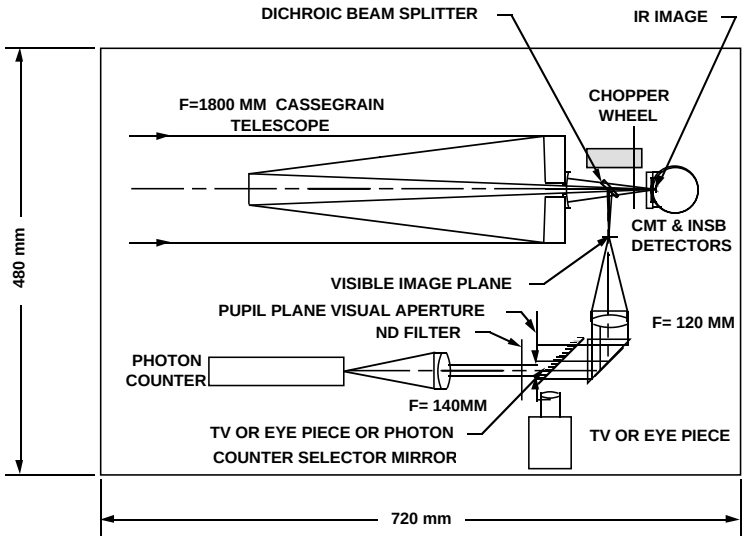

Figure 2. Collection optics schematic.

2.3. Data acquisition and processing system

The InSb and CMT detectors produce a pair of analogue output signals. These signals are fed, via a pre-amp, to a Data Translation multi-channel analogue-to-digital converter board (DT3001). The CO_2 laser is chopped at approximately 434Hz and a similar value is used for the extended source with the Cassegrain optics: the IR signals are filtered to prevent aliasing with a smooth roll-off filter (designed and constructed by Dr A Cañas) with a nominal cut-off of 800Hz. The Data Translation board is controlled by a Dell Pentium II PC. The board is programmed to acquire large blocks (16K or 32K points) of data at user-selectable intervals. The overall control of the data acquisition process is via a Visual C++ program running in the NT based computer. Data blocks are acquired from the IR detector, and saved to a local disk or CD. All data is archived on CD.

It was found whilst developing the acquisition system that the photon counting signal could not be controlled by the same DT acquisition board. The photon counting signal is therefore acquired by a EMI photon counting card, Model C660/CT1, capabable of a peak count rate of 20MHz (i.e. 50ns deadtime). The board is controlled by a Toshiba 4400 and can be programmed to count at intervals of 12μs to 30sec. The two computers are linked via a serial line (RS232)and a local ethernet (10BaseT) . The Visual C++ program transmits the acquisition parameters via the serial line, once acknowledged a go signal is sent. Once the IR signals are successfully acquired by the Dell computer, the Toshiba is checked to ensure the photon counting signal has been acquired. Once acquired, the data is transferred to the Dell via TCP/IP.

Given that the deadtime of the photon-counting system is nominally 50ns (i.e. 20Mhz peak count rate), in order not to bias the moments of the intensity, the average count rate should be kept below 200Kz (i.e. less than 1000 per 0.5ms sample time) and in practice we keep below an average of 100 per sample time. On the other hand, the average photon count rates are sufficiently large that the differences between histograms for photon counts and classical intensity can be safely ignored.

2.4. Observations

Measurements over a 17.55km path between Bredon Hill (maintained by DERA Defford) and DERA Malvern were made in November 97, February 1998, April 1998, July 1998 and September 1998.

Data was collected in all three wavelength channels simultaneously, the long-wavelength IR data originating either from the CO_2 laser or from the extended source. A typical run involves the collection of 20 sets of 16,000 samples

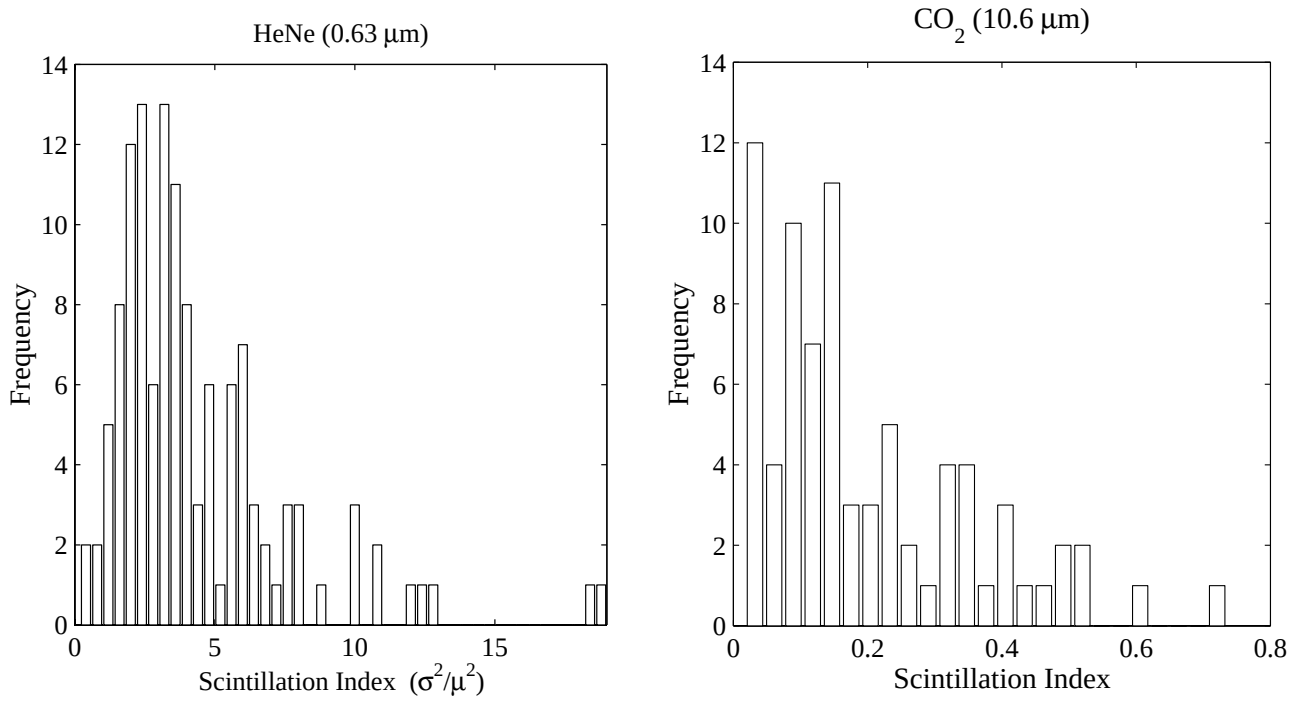

Figure 3. Left: Normalised variance (or scintillation index) frequency distribution at a wavelength of 633nm, measured over approximately 130 samples (the extreme single value of ≈34 is not plotted). Right: Normalised variance (or scintillation index) frequency distribution at a wavelength of 10.6μm, measured over approximately 78 samples.

(i.e. 320,000 samples) at 2Khz sampling rate for the visible channel and 20 sets of 32,000 samples (i.e. 650,000 samples) at 4Khz sampling rate for the IR channels. Virtually all data has been collected during daytime hours.

The original data was recorded for archival purposes on CD ROMs, and the reduced data plus weather information and pictures are available as a CD, readable using a WWW-browser. The three principal quantities calculated from the data are:

- The histogram of intensities for each detector signal (plotted on linear and logarithmic scales), together with the predicted curves for various theoretical models (log-normal, exponential, log-normally modulated exponential, K distribution).
- The power spectral densities for each detector signal.
- The autocorrelation function for each detector signal, with an equivalent bandwidth marked.

The recorded data naturally has some degree of spatial and temporal averaging, although the latter is small due to the short sampling times used. This averaging has to be taken into account in the interpretation of the data.

3. RESULTS

3.1. Variance

The normalised variance is defined by

$$\sigma_I^2 = \frac{\langle I^2 \rangle - \langle I \rangle^2}{\langle I \rangle^2} \tag{1}$$

where $\langle I^2 \rangle$ is the second moment and $\langle I \rangle$ is the mean. For *weak* turbulence, the normalised variance over a statistically uniform path of length Z is given by

$$\sigma_I^2 \approx 1.2\ C_n^2\ k^{7/6}\ Z^{11/6} \tag{2}$$

where C_n^2 is the refractive index structure constant and $k = 2\pi/\lambda$. The variance of scintillation index or normalised variance varies as $\lambda^{-7/6}$, and thus, for *weak* turbulence, we would expect the variance to be approximately 27 times smaller at 10.6μm (CO_2 wavelength) than at 633nm (He-Ne wavelength), assuming the same degree of detector (spatial and temporal) integration.

Figure 3 summarises the measurements of the normalised variance for the He-Ne and CO_2 laser results. For the He-Ne (λ = 633nm), $\sigma_I^2 = 4.8 \pm 4.1$, and for the CO_2 ($\lambda = 10.6\mu$m), $\sigma_I^2 = 1.2 \pm 1.4$. The measurement apertures were of diameter 6 and 150mm respectively, i.e. there was a greater degree of spatial integration at the CO_2 laser wavelength.

As one might expect, there is a very great variation in the normalised variance over the data set, the variance itself having a form that is approximately log-normal. Values up to approximately 5-6 should be consistent with simulation results for a point source if a reasonable value for the inner scale is substituted but it would appear to be difficult to explain values of the normalised variance greater than approximately 6 by extrapolations of our own simulation results or by those presented in the literature.[8–10] It should also be borne in mind that our measurements also involve some degree of spatial and temporal averaging, making them lower than those predicted from simulations which ignore such averaging effects.

It is important to emphasise that our results are the first such results published in the open literature, and that previous theoretical and simulation studies have not had the challenge of explaining such large measured values of the normalised variance. Clearly further studies are required, either to explain why we measured such large values or to prove that they are "impossible". For example, could non-Kolmogorov effects, perhaps associated with intermittancy, explain our results?

3.2. Probability Density

For weak turbulence, the argument leading the probability density function is as follows: the wave propagates through many independent turbulence cells, each having a multiplicative effect on the wave complex amplitude (additions in the exponent), and thus, by the central limit theorem, the induced fluctuations are log-normal. Although for weak turbulence there is a theoretical prediction for the normalised variance σ_I^2 of the intensity (the only free parameter), in general we treat σ_I^2 as a fitting parameter.

The log-normal distribution $[p(I)]_{LN}$ is defined by:

$$[p(I)]_{LN} = \frac{1}{\gamma I\sqrt{2\pi}} \exp\left(-\frac{(\ln I - < \ln I >)^2}{2\gamma^2}\right)$$

where γ^2 is the variance of the natural logarithm of the intensity. The variance of the intensity σ_I^2 is related to γ^2 by

$$\sigma_I^2 = \exp(\gamma^2) - 1$$

The log-normally modulated exponential probability density function, $[p(I)]_{LNME}$, was first proposed by Churnside and Hill[11] for strong fluctuations, on the basis that it provided "excellent agreement with the data". It is given by

$$[p(I)]_{LNME} = \frac{1}{\sigma_z\sqrt{2\pi}} \int_0^\infty \exp\left(-\frac{I}{z} - \frac{(\ln z + \frac{1}{2}\sigma_z^2)^2}{2\sigma_z^2}\right)\frac{1}{z^2}dz$$

where σ_z^2 is the variance of the modulation of the expontial component. It can be shown that this is related to the variance of the intensity σ_I^2 by

$$\sigma_I^2 = 2\sigma_z^2 - 1$$

where it should be noted that $\sigma_I^2 \geq 1$.

The K probability density function, $[p(I)]_K$, was first proposed by Jakeman and Pusey[12] for fitting data that physically were a result of a random walk with a variable number of steps. It is given by

$$[p(I)]_K = \frac{2}{\Gamma(y)} y^{y(y+1)/2} I^{(y-1)/2} K_{y-1}\left((2\sqrt{Iy}\right)$$

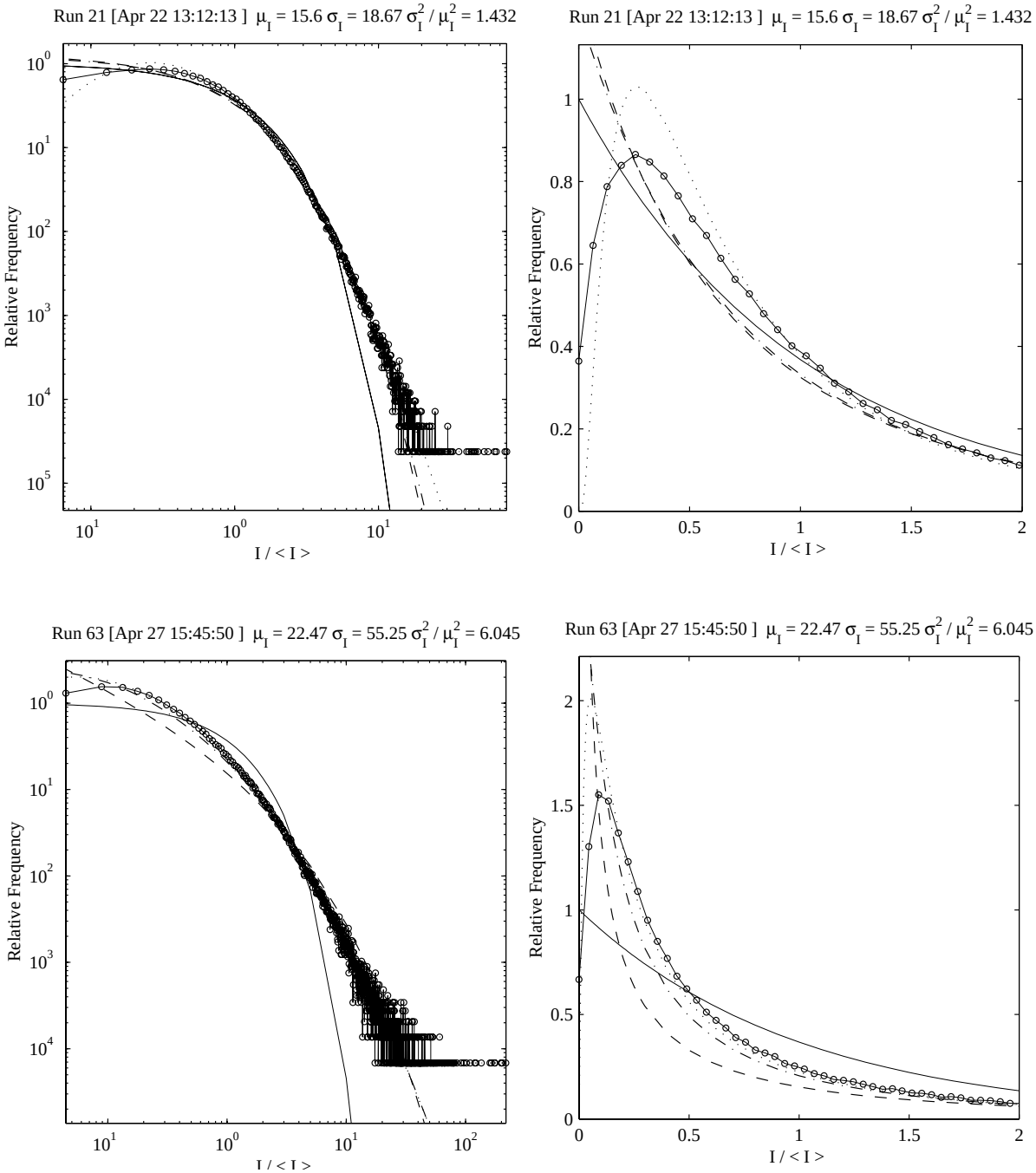

Figure 4. Histograms (log scale on left, linear scale on right) for the intensity fluctuation for visible point source data, for values of the normalised variance of ≈1.4 (top) and ≈6.0 (lower). The solid line joined by circles is the measured data, the solid line (without circles) is the exponential fit, the dotted line is the log normal fit, the dashed line is the K distribution fit and the dot-dashed is the log normally modulated exponential fit. The theoretical curves are fitted using the measured normalised variance.

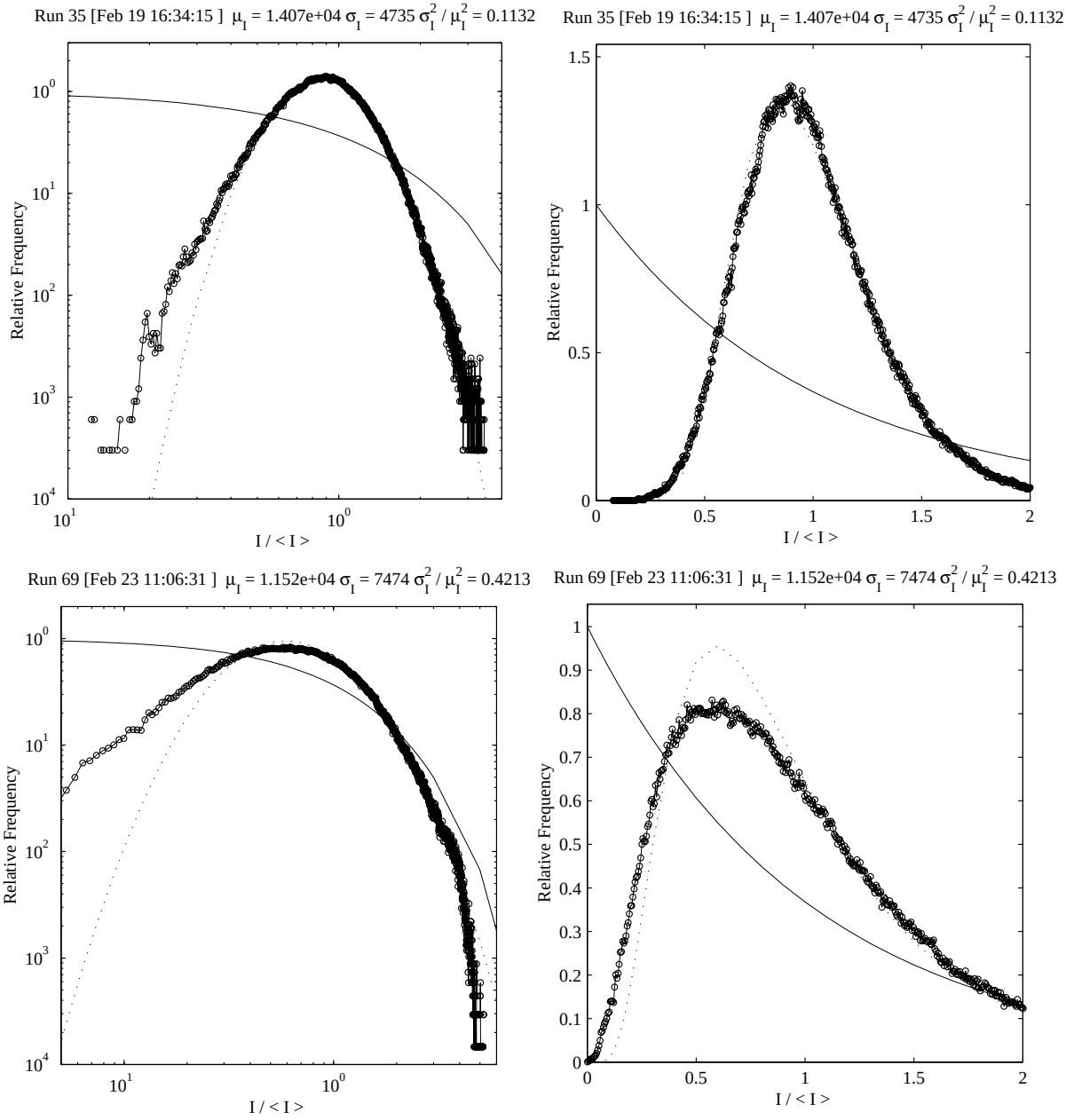

Figure 5. Histograms (log scale on left, linear scale on right) for the intensity fluctuation for CO_2 10.6μm point source data, for values of the normalised variance of ≈0.11 (top) and ≈0.42 (lower). The solid line joined by circles is the measured data, the solid line (without circles) is the exponential fit (of no practical interest here) and the dotted line is the log normal fit; note the excellent fit to the log-normal distribution for the low-variance (upper) case.

where $K_\nu(x)$ is the modified Bessel function. The variance of the intensity σ_I^2 is related to the parameter y by

$$\sigma_I^2 = \frac{2}{y} + 1$$

where it should be noted that $\sigma_I^2 \geq 1$.

Finally, in the limit of very strong turbulence, it is expected that a fully developed speckle pattern would be formed, giving a negative exponentially distributed probability density function: this is defined by its mean value, with a normalised variance of unity.

Figures 4 and 5 show four of the 350 histograms measured, for visible (Fig.4) and 10.6μm (Fig.5), together with fits to the various models based on the value of the normalised variance. Despite a detailed examination of the whole dataset, we cannot be make definitive statements about the best fit distributions, except to say that the log-normal distribution, which is a very good fit for small values of the normalised variance, apparently also fits quite well when the fluctuations are larger. At *very* large values of the normalised variance, greater than approximately five, none of the suggested distributions appears to give a good fit. Of course, such large variances could be the result of non-stationary effects but we have observed that high variances can occur when second order stationarity appears to hold.

Clearly there is scope for further analysis of this very extensive dataset. The problems posed by having a finite number of samples has been explored by other authors[13,14] and in this connection the use of fractional moments has been suggested.[15] There are some fundamental issues in the analysis of large-variance data.[16]

3.3. Power Spectra and Correlation Functions

Figure 6 shows the power spectra and autocorrelation functions for the same data shown in Fig.5, the the CO_2 laser source. We prefer to work with mainly the correlation functions, since these give a more direct physical understanding of the temporal characteristics of the processes. The correlation time is defined as shown on the lower part of Figure 6, where the area of the rectangle defining the correlation time is the same as that of the measured correlation function.

Figure 7 shows histograms of the correlation time for all the visible and 10.6μm data. The average correlation time for Ne-He radiation ($\lambda = 633$nm) was 9.8$\pm$4.8ms, whereas for 10.6μm it was 68$\pm$39ms.

4. CONCLUSION

A large body of scintillation data has been collected and analysed at three wavebands using both laser sources and an extended source over a 17.55km horizontal path. Scintillation data in the visible shows some remarkably large values for the normalised variance, and existing models do not provide a good fit to the measured histograms for these very large variance cases. For more modest values of the normalised variance, the log-normal distribution appears to provide a good fit beyond the low-variance regime where it is well-known to provide the best fit. The analysis of high variance scintillation data deserves further study, since there are number of fundamental difficulties to be resolved.

ACKNOWLEDGMENTS

This project was funded by the UK Defence Evaluation Research Agency (DERA) under Contact ASF/3007.

REFERENCES

1. G. R. Ochs, R. R. Bergman, and J. R. Snyder, "Laser-beam scintillation over horizontal paths from 5.5 to 145 kilometers," *J Opt Soc Am* **59**, pp. 231–234, 1969.
2. J. H. Churnside and R. G. Frehlich, "Experimental evaluation of log-normally modulated rician and IK models of optical scintillation in the atmosphere," *J Opt Soc Am A* **6**, pp. 1760–1766, 1989.
3. A. Consortini, F. Cochetti, J. H. Churnside, and R. J. Hill, "Inner-scale effect on irradiance variance measured for weak-to-strong atmospheric scintillation," *J Opt Soc Am A* **10**, pp. 2354–2362, 1993.
4. D. Dravins, L. Lindegren, E. Mezey, and A. T. Young, "Atmospheric intensity scintillation of stars 1. Statistical distributions and temporal properties," *Publ Astr Soc Pac* **109**, pp. 173–207, 1997.

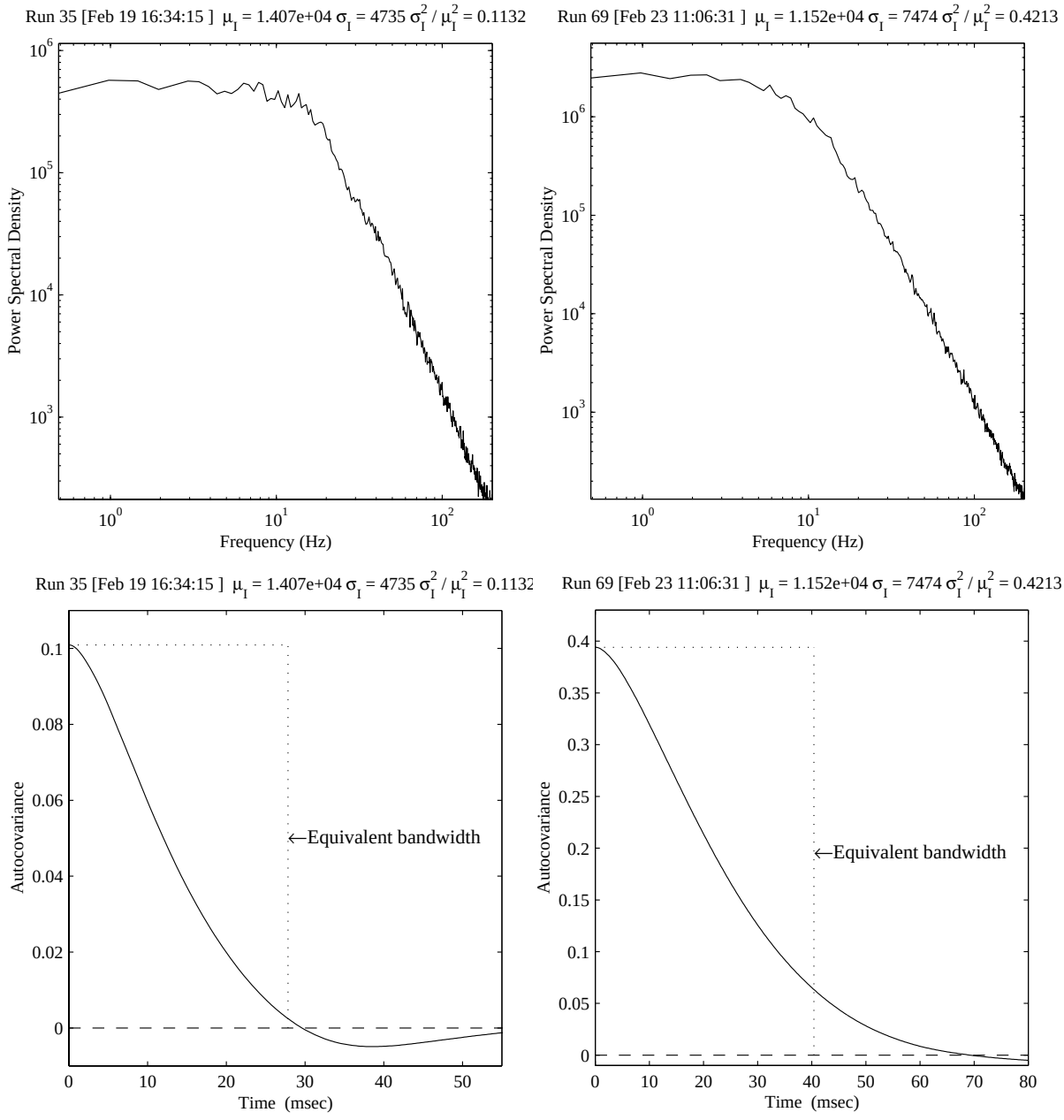

Figure 6. Power spectra and correlation functions for the data sets of Figure 5 (CO_2).

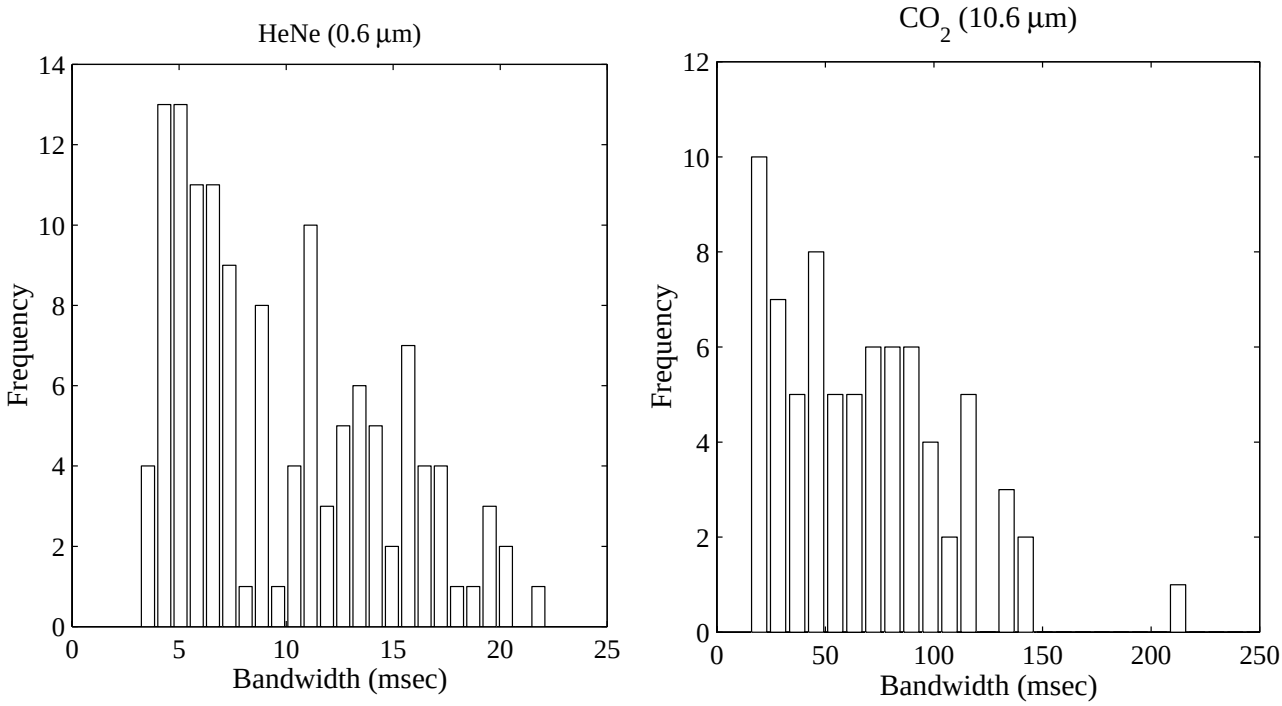

Figure 7. Left: Histogram of the correlation time (as defined in the text) for the He-Ne (633nm) dataset of 130 results. Right: Histogram of the correlation time (as defined in Fig. 6) for the CO_2 (10.6μm) dataset of 78 results.

5. D. Dravins, L. Lindegren, E. Mezey, and A. T. Young, "Atmospheric intensity scintillation of stars 2. Dependence on optical wavelength," *Publ Astr Soc Pac* **109**, pp. 725–737, 1997.
6. D. Dravins, L. Lindegren, E. Mezey, and A. T. Young, "Atmospheric intensity scintillation of stars 3. Effects for different telescope apertures," *Publ Astr Soc Pac* **110**, pp. 610–633, 1998.
7. D. L. Hutt, "Modelling and measurements of atmospheric optical turbulence over land," *Opt Engng* **38**, pp. 1288–1295, 1999.
8. S. M. Flatté, G.-Y. Wang, and J. Martin, "Irradiance variance of optical waves through atmospheric turbulence by numerical simulation and comparison with experiment," *J Opt Soc Am A* **10**, pp. 2363–2370, 1993.
9. S. M. Flatté, C. Bracher, and G.-Y. Wang, "Probability density functions of irradiance for waves in atmospheric turbulence calculated by numerical simulation," *J Opt Soc Am A* **11**, pp. 2080–2092, 1994.
10. W. A. Coles, J. P. Filice, R. G. Frehlich, and M. Yadlowsky, "Simulation of wave propagation in three-dimensional random media," *Applied Optics* **34**, pp. 2089–2101, 1995.
11. J. H. Churnside and R. Hill, "Probability density of irradiance scintillations for strong path-integrated refractive index turbulence," *J Opt Soc Am A* **4**, pp. 727–733, 1987.
12. E. Jakeman and P. N. Pusey, "A model for non-Rayleigh sea echo," *IEEE Trans Antennas Prop* **AP-24**, pp. 806–814, 1976.
13. N. Ben-Yosef and E. Goldner, "Sample size influence on optical scintillation analysis 1: Analytical treatment of the higher order moments," *Appl Opt* **27**, pp. 2167–2171, 1988.
14. E. Goldner and N. Ben-Yosef, "Sample size influence on optical scintillation analysis 2: Simulation approach," *Appl Opt* **27**, pp. 2172–2177, 1988.
15. A. Consortini and F. Rigal, "Fractional moments and their usefulness in atmospheric laser scintillation," *Pure Appl Opt* **7**, pp. 1013–1032, 1998.
16. R. J. Hill and J. H. Churnside, "Observational challenges of strong scintillations or irradiance," *J Opt Soc Am A* **5**, pp. 445–447, 1988.